Chinese Chemical Letters 36 (2025) 110169

Contents lists available at ScienceDirect

Chinese Chemical Letters

journal homepage: www.elsevier.com/locate/cclet

A self-powered cathodic molecular imprinting ultrasensitive photoelectrochemical tetracycline sensor *via* ZnO/C photoanode signal amplification

Qinghong Pan[a], Huafang Zhang[a], Qiaoling Liu[b], Donghong Huang[b], Da-Peng Yang[a,b,c,*], Tianjia Jiang[c], Shuyang Sun[d], Xiangrong Chen[b,*]

[a] *Key Laboratory of Chemical Materials and Green Nanotechnology, College of Chemical Engineering and Materials Science, Quanzhou Normal University, Quanzhou 362000, China*
[b] *Department of Neurosurgery, the Second Affiliated Hospital of Fujian Medical University, Quanzhou 362000, China*
[c] *School of Rehabilitation Science and Engineering, University of Health and Rehabilitation Sciences, Qingdao 266024, China*
[d] *College of Food Engineering, Ludong University, Yantai 264025, China*

ARTICLE INFO

Article history:
Received 10 January 2024
Revised 11 June 2024
Accepted 21 June 2024
Available online 22 June 2024

Keywords:
Self-powered photoelectrochemical sensor
Molecularly imprinted polymer
Fe-doped $CuBi_2O_4$
Tetracycline detection

ABSTRACT

Quantitative determination of tetracycline (TC) in environment and foods is of great importance, as excessive residues might have negative effects on human health and environmental risks. Herein, a self-powered molecularly imprinted photoelectrochemical (PEC) sensor based on the ZnO/C photoanode and the Fe-doped $CuBi_2O_4$ (CBFO) photocathode is developed for the sensitive detection of TC. The photocathodic current can be amplified by the efficient electron transfer caused by the Fermi energy level gap between the photoanode and photocathode. Furthermore, molecularly imprinted polymers (MIPs) at photocathode can selectivity identify the TC templates and thus improve the specificity. Under the optimal conditions, the sensor has a linear range of 10^{-2}–1.0×10^5 nmol/L, and a limit of detection (LOD) of 0.007 nmol/L (S/N = 3). More crucially, the milk sample detection is carried out using the as-prepared sensor, and the outcome is satisfactory. The research gives us a novel sensing platform for quick and accurate antibiotic (like TC) in environment and food monitoring.

Antibiotics, as a type of secondary metabolites naturally produced by microorganisms, can be synthesized chemically or semi-synthetically into analogous molecules. Because of their potent antibacterial properties, antibiotics have been widely employed in the prevention and treatment of human and animal infectious diseases [1], as well as the stimulation of animal growth [2,3].

Tetracycline (TC), an antibiotic with broad-spectrum antibacterial action, is frequently used to prevent and treat the different bacterially-caused diseases that affect animals [4,5]. Tetracycline is used to cure diseases as well as to enhance animal growth, which increases the danger of TC residues in animal products posing a health concern to humans [6,7]. Additionally, due to the slow degradation rate of TC, it eventually can reach the natural environment through a variety of channels, including rivers, soil, agricultural, and industrial effluent. The ideal concentration level of TC residues in food has been defined by many organizations and nations to assure consumer safety [8,9]. For example, Food and Agriculture Organization of the United Nations (FAO) and World health Organization (WHO) have set the maximum residue limit for TC in milk as 100 mg/L, while the US Food and Drug Administration (FDA) has set the safety standard for TC, oxytetracycline and cholortetracycline in milk as 80, 30 and 30 mg/L [10], respectively. The amount of tetracycline in meat is limited to 100 mg/kg in China [4]. In addition to trace amounts of TC in food, trace amounts of TC have also been detected in industrial wastewater outlets and soil watered by manure in China and foreign countries such as the United States. Up to now, several conventional methods including high-performance liquid chromatography (HPLC) [11], liquid chromatography-mass spectrometry (LC-MS) [12], capillary electrophoresis (CE) [13] and fluorescent sensing [14] have been reported for the detection of TC. However, traditional methods have a number of drawbacks that make them unsuitable for field testing, including expensive equipment, specialised operators, laborious and time-consuming sample preparation procedures, and multi-step cleaning. Therefore, it is necessary

* Corresponding authors.
E-mail addresses: yangdp@qztc.edu.cn (D.-P. Yang), xiangrong_chen281@126.c (X. Chen).

https://doi.org/10.1016/j.cclet.2024.110169
1001-8417/

to develop a simple, sensitive, accurate and energy-saving detection method for TC in environment [15].

Photoelectrochemical (PEC) sensing as a new technology was developed from electrochemical techniques [16], which has garnered a lot of attention for its straightforward instrument, low background signal, and quick response times [17]. In recent years, PEC sensing system has been widely used for the detection of environmental pollutants and drugs [18], and the food safety monitoring [19]. As opposed to electrochemical sensing, PEC measurements are typically performed in an "optical excitation-electrical detection" mode, where the light source and the detection signal are entirely distinct and in different energy forms with a higher sensitivity because of the significantly reduced background signals [20]. For the traditional PEC analysis, a three-electrode electrochemical system is usually used for detection, wherein the photoelectrode, Pt wire and Ag/AgCl or saturated calomel electrode (SCE) are used as the working electrode (WE), the counter electrode (CE) and the reference electrode (RE), respectively [21]. However, since the conventional photoelectrode is worked as both the signal source and sensing platform, the reducing chemicals in actual samples might easily interfere with the detection performance of such sensors [22]. In light of this, the self-powered photoelectrochemical sensor system is developed by substituting the CE in the conventional three-electrode system with the photoanode, the WE in place of the photocathode, and Ag/AgCl or SCE in place of the RE in the absence of an external power source [9]. In this instance, the photoanode is utilised to amplify the photoelectric signal while a photocathode is solely employed for sensing analysis. The electrical signal is produced by the potential difference between the photoanode and the photocathode [23]. This type of self-powered PEC sensing technique can be used as a powerful instrument to deliver the high sensitivity, selectivity, and remarkable precision needed to find crucial targets [24].

Photoactive materials with significant photoelectric effect play an important role in self-powered PEC sensors [25]. When the photoactive material is subjected to stimulating light, it can produce electrons-holes pair, and the photocurrent that results from charge transfer is produced as a detecting signal [26]. Nowadays, semiconductor materials as excellent photoactive materials have been widely studied [27], including n-type semiconductor with electron as carrier and p-type semiconductor with holes as carrier [28]. Zinc oxide (ZnO), a typical n-type semiconductor with exceptional characteristics, is regarded as a superior photocatalyst due to its low cost and simplicity of manufacture [29,30]. However, due to its wide band gap, its optical response range is limited [31], the introduction of carbon can improve the photoelectric properties of ZnO, reduce the band gap and prolong the carrier lifetime [32]. Therefore, ZnO/C is used as photoanode to provide electrons in the self-powered PEC system. Furthermore, $CuBi_2O_4$ (CBO), as a member of Cu-based oxides photocathodes, have received a great deal of interest due to a narrow-gap and relatively good conductivity [33]. While the pure CBO photocathode has poor photoelectric performance, limited carrier mobility, and facile electron-hole recombination [33]. To solve these problems, external element doping was introduced to improve the PEC performance of the CBO photocathode, where the doping-element substitutionally replaced Bi^{3+} ions [34]. Virtually, introduction of dopants will increase the concentration of holes in the bulk, showing the enhancements of photocurrent intensity and stability, the introduction of Fe^{3+} will replace the Bi^{3+}, and increase the number of electron hole pairs, thus increasing the electron transfer rate [35]. Therefore, Fe-doped $CuBi_2O_4$ (CBFO) will be beneficial to improve PEC performance of the photocathode [36].

Recognition element is a crucial component of a PEC sensor. Molecularly imprinted polymers (MIPs), known as "artificial antibodies" [37], are created by combining cross-linked monomers and functional polymeric monomers in the presence of template molecules [38,39]. Compared with traditional recognition components (antibodies, aptamers, *etc.*) [40], MIPs have the advantages of low cost, excellent chemical stability, high sensitivity and so on. In recent years, MIPs have been widely utilized in chromatographic separation, drug delivery, bioimaging, and other applications [41,42]. As a result, molecularly imprinted polymer technology, used as the recognition component of PEC sensors, can specifically recognize the target molecule, considerably enhancing the sensor's selectivity [14].

In this work, a self-powered molecular imprinted PEC sensor is developed for the sensitive determination of TC, in which the photoanode (ZnO/C) is combined with the photocathode (CBFO) to promote photocurrent generation for the first time without adding electron donors or acceptors to the system. As can be seen in Scheme S1 (Supporting information), ZnO/C composite nanomaterials obtained through high temperature calcination is employed as the photoanode [43], while CBFO prepared *via* the electrodeposition and annealing process is used as the photocathode with an Ag/AgCl electrode worked as reference electrode to construct a self-powered sensor system. The electrons of the photoanode can be transferred to the photocathode under light irradiation and are attracted by the holes in the photocathode, generating an electric current without bias and extra electron acceptors. The molecularly imprinted polymer film on the photocathode can selectively identify the TC molecules, change the photocurrent response, and realize the sensitive detection of TC, while avoiding the interference of the reducing substances in the sample and complex biometric reaction. The experimental findings demonstrate the built-in PEC sensor's high sensitivity, good stability, and outstanding selectivity, which exhibits reasonable TC detection performance in the wastewater and milk samples, demonstrating sensor detection's tremendous potential.

All reagents are analytical grade and can be used without further purification. Tetracycline (TC), oxytetracycline (OTC), chlortetracycline (CTC), chloramphenicol (CAP), kanamycin (KAN), erythromycin (ERY), zinc gluconate hexahydrate ($C_{12}H_{22}O_{14}Zn{\cdot}xH_2O$, 98%), bismuth nitrate pentahydrate, copper nitrate trihydrate and iron nitrate ninehydrate were purchased from Aladdin (Shanghai, China). Acetic acid, ethanol, acetone, methanol, anhydrous sodium sulfate, potassium chloride, sodium acetate, disodium hydrogen pgosphate, ethylenediaminetetraacetic acid disodium salt, nitric acid and 5% Nafion®117 solution were provided by Sinopharm Chemical Reagent Co., Ltd. Potassium ferricyanide, potassium hexacyanoferrate, *o*-phenylenediamine ($C_6H_4(NH_3)_2$) (*o*-PD) were obtained from Shanghai Macklin Biochemical Co., Ltd. The milk sample was purchased from Yonghui Supermarket. Ultrapure water (18.25 MΩ cm) was obtained from a Milli-Q system.

The microstructure and morphology of the samples were explored with scanning electron microscope (SEM, Zeiss, Germany) with in situ elemental analysis *via* energy dispersive spectrometer (EDS). The crystal structures of the prepared samples were characterized by X-ray diffraction (XRD, Bruker (D8 Advanced)) using Cu Kα radiation generated at 40 kV and 40 mA, and the corresponding patterns were recorded in the range of 5° to 80° (2θ) with a scanning step of 10° min^{-1}. The surface functional groups of the prepared materials were studied *via* a Fourier transform infrared (FT-IR) spectrometer (Nicolet iS 50 FT-IR, Thermo Scientific, USA). The elemental analyses of the samples were performed on an X-ray photoelectron spectrometer (XPS, Kratos Axis Ultra DLD). The PEC measurementswere conducted by using a three-electrode system with a 70 W metal halide lamp as the light source. A three-electrode system was adopted by using FTO electrodes ($10 \times 50 \times 2.2\,mm^3$) (South China Xiangcheng Technology Co., Ltd.) as the photoanode and the photocathode, and a calomel electrode as the reference electrode. The optoelectronic

data were recorded by using an electrochemical workstation (CHI 660E).

Through high-temperature calcination, the ZnO/C composite nanomaterials were created using a green chemical process. A certain amount of zinc gluconate samples was calcined in a crucible at 700 °C in nitrogen atmosphere for 3 h. The resulting powder samples were labeled as ZnO/C and ground into a fine powder using an agate mortar, and then stored for further use. Prior to preparation of the photoanode, the FTO electrodes were ultrasonically cleaned with acetone, ethanol, and ultrapure water for 10 min successively and dried. The working electrode was covered with an insulating transparent tape to control the fixed exposure area of 10 mm × 10 mm. Next, 40 mg of ZnO/C material, 40 μL of Nafion solution and 2 mL of isopropanol solution were mixed uniformly in a 10 mL centrifugal tube with ultrasonic bath for 10 min. The active layer of the treated FTO electrode was immersed in the mixed solution. The ZnO/C-FTO electrode was prepared by repeating the above-mentioned process successively for 3–4 times.

The CBFO films modified FTO electrodes were prepared by the electrodeposition and annealing as described before [44]. Firstly, the FTO electrodes were ultrasonically cleaned with acetone, ethanol, and ultrapure water successively for 10 min and dried. 6.0 mmol/L $Bi(NO_3)_3$ $5H_2O$, 4.0 mmol/L $Cu(NO_3)_2{\cdot}3H_2O$ and 2.0 mmol/L $Fe(NO_3)_3{\cdot}9H_2O$ were added into 10% HNO_3 solution to form the precursor solution. After that, the treated FTO was put into the precursor solution, deposited at constant potential −0.5 V for 150 s, and then rinsed with deionized water. Finally, the Fe-doped $CuBi_2O_4$-FTO (CBFO-FTO) was successfully synthesized by calcination in a muffle furnace at 450 °C for 2 h with a surface color change from black to dark brown.

In order to prepare molecularly imprinted polymer (MIP), 0.5 mmol/L *o*-PD and 0.5 mmol/L TC were added into 100 mL 0.2 mol/L phosphate buffer solution (PBS) to prepare MIP preparatory solution. The electrodeposition of MIP on the surface of the CBFO-FTO electrode were carried out with cyclic voltammetry (CV) at a scan rate of 50 mV/s in the potential range of 0–0.8 V (*vs.* Ag/AgCl)in the MIP preparatory solution with 30 cycles. The obtained electrodes were washed alternately with ethanol and distilled water and dried at room temperature to obtain the CBFO/MIP-FTO electrode. The non-imprinted polymer modified the CBFO-FTO electrodes (CBFO/NIP-FTO) was prepared under the above-mentioned conditions except for omission of the TC template. The CBFO/MIP-FTO electrode was immersed in a mixture of methanol and acetic acid (v:v = 9:1) to elution the TC template molecules to obtain the CBFO/rMIP-FTO electrode for the detection of TC.

The self-powered PEC sensor experiment was carried out in 0.2 mol/L Na_2SO_4 solution. Under a potential of 0 V, with the ZnO/C-FTO electrode as the photoanode, the CBFO/rMIP-FTO electrode as the photocathode, and a calomel electrode as the reference electrode, the current-time curve was recorded with the light being switched on successively for 20 s. Electrochemical impedance spectroscopy (EIS) was studied in 0.1 mol/L KCl solution containing 0.1 mmol/L $K_3[Fe(CN)_6]$ and 1 nmol/L $K_4[Fe(CN)_6]$ under dark conditions.

According to the previously reported pretreatment method for milk samples [45]. 2 mL of milk samples obtained in the local market were taken into a beaker, 8 mL of Na_2EDTA-McIlvaine buffer solution was added, and ultrasonically mixed. The mixture was centrifuged twice for 15 min, filtered three times with a 0.45 μm ultrafiltration membrane, and refrigerated for later use. Because the milk bought from the market is antibiotic-free, different concentrations of TC were added to the milk samples to illustrate the proposed sensor's accuracy in practical analysis.

The microstructure of the different electrode materials were investigated by SEM. As shown in Figs. 1A-C, the ZnO particles exhibit the uniform distribution on the carbon surface, indicating that the addition of carbon can lead to the improved dispersion of the ZnO particles and increase their contact area (Fig. S1 in Supporting information). As shown in Figs. 1D-F, the CBFO composite shows irregular nanoparticle-like structures with large surface areas. These CBFO nanoparticles are distributed uniformly on the surface of the FTO electrode. The EDS was used for further characterization of the ZnO/C and CBFO composite, the elements are appeared in the elemental mappings (Figs. S2 and S3 in Supporting information), suggesting the successful preparation of this composite.

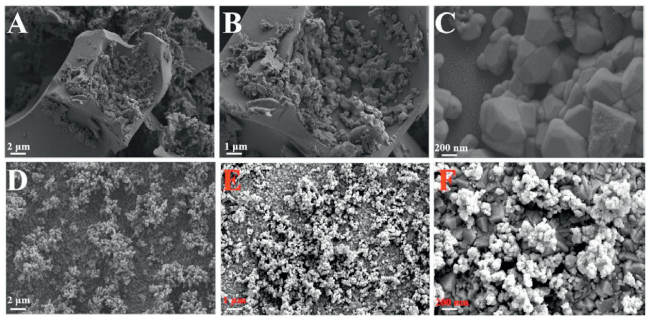

Fig. 1. SEM images of (A-C) the photoanode ZnO/C and (D-F) photocathode CBFO.

The XRD analysis was implemented to analyze the crystal structures and phase compositions of different materials. The XRD pattern of the ZnO/C material is perfectly indexed to the pattern for ZnO (JCPDS No. 238 79–0208) (Fig. S4A in Supporting information) [46]. Fig. S3B shows the characteristic diffraction peaks of CBO (red heart) at 21.4°, 27.7°, 33.1°, 37.4°, 46.4°, 52.8° and 55.4°, which could be indexed to (200), (211), (310), (202), (411), (213) and (332) planes (PDF #48–1886) [44]. According to the XRD pattern of CBFO (black line), there is no characteristic peak related to Fe, indicating that the doping of Fe element has no effect on the crystal structure.

The surface elemental composition and valence states of the ZnO/C and CBFO materials were characterized by XPS. As shown in Fig. S4C (Supporting information), the full XPS spectrum of the ZnO/C material reveals the presence of Zn, O, and C elements. As illustrated in Fig. S5A (Supporting information), two noticeable peaks are appeared in the Zn 2p XPS spectrum located at 1022.6 and 1045.6 eV, which are ascribed to the $2p_{3/2}$ and $2p_{1/2}$ peaks of Zn^{2+}, confirming the presence of zinc ions. According to the Gaussian fitting results, the XPS peaks at 531.4 and 532.6 eV referring to the Zn-O-C/-OH and carbonate (C–O/C=O) groups can be observed in the XPS spectrum of O 1s, respectively (Fig. S5B in Supporting information). In the high-resolution C 1s spectrum (Fig. S5C in Supporting information), three peaks at 284.8, 285.6 and 288.9 eV, were attributed to the C–C bond, Zn-O-C bond, and C=O bond, respectively. The results confirmed the presence of zinc ions. As shown in Fig. S4D (Supporting information), the full XPS spectrum of CBFO reveals the presence of Cu, Fe, O and Bi elements. For Cu 2p spectrum (Fig. S6A in Supporting information), the peaks of Cu $2p_{3/2}$ and $2p_{1/2}$ located at 933.7 and 953.5 eV, proving the existence of Cu^{2+}.The Bi 4f spectrum (Fig. S6B in Supporting information) revealed two characteristic peaks of 158.8 and 164.1 eV, were associated with $4f_{7/2}$ and $4f_{5/2}$ orbitals of Bi^{3+} in the CBFO composite. The high-resolution Fe 2p spectra was shown in Fig. S4C. These results prove the successful synthesis of the materials for photoanode and photocathode.

To validate the successful construction of sensing photocathode, the chemical bonds were analyzed by FT-IR spectroscopy (Fig. S7 in Supporting information). The characteristic peaks of 2927 cm^{-1} are ascribed to stretching vibration of C–H bonds, and the FT-IR

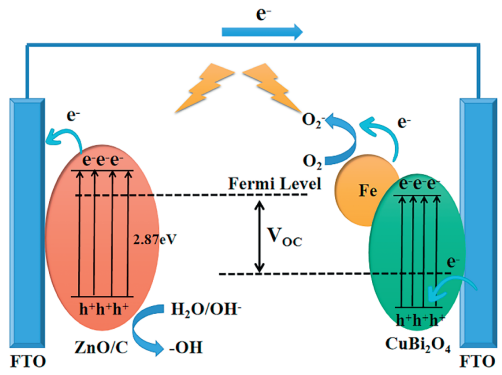

Scheme 1. Mechanism of the self-powered photoelectrochemical sensor system.

band of CBFO appears at 519 cm^{-1} due to the stretching vibration of Bi-O bonds and Cu-O bonds. Furthermore, the FT-IR spectra of the CBFO/MIP electrode before and after the removal of template were analyzed to characterize. The characteristic peak at 1636 cm^{-1} corresponds to the stretching vibration of the carbon-carbon double bond (C=C) on the benzene ring, and the characteristic peak at 3443 cm^{-1} corresponds to the stretching vibration of the hydroxyl group (O–H) of the amino group and the nitro-hydrogen bond (N–H), which is consistent with the previously reported, indicating the successful electropolymerization of *o*-PD [45]. In addition to the above peaks, the peak at 1284 cm^{-1} indicates that CBFO/MIP is different from CBFO/rMIP and CBFO/NIP, which may be related to the polymerization form of TC molecules with *o*-PD. These FT-IR results further verified the successfully preparation of the molecularly imprinted sensor.

Since the Fermi energy levels of n-type semiconductors are close to the conduction band (CB), while the Fermi energy levels of p-type semiconductors are close to the valence band (VB), such a significant deviation between the Fermi levels of photo-anode and photocathode is considered to be the main driving force for generating photocurrent in this system. The detailed mechanism is shown in Scheme 1. When the system is exposed to the visible light, the photo-induced electrons can be diverted from the ZnO/C to photocathode with the aid of external circuit, further being captured by O_2 dissolved in the electrolyte. Meanwhile, the holes are transferred in opposite directions, which were reduced by H_2O at photoanode.

At the same time, the CBFO on the photocathode captures the electrons from the photoanode, and the introduction of Fe^{3+} makes the electron transfer rate faster, thus making the redox reaction of the system faster. When the TC binds to the specific recognition site on the photocathode, photo-induced electrons are prevented from reacting with O_2 due to the increased steric hindrance, leading to generation of a reduced photocurrent. The possible reaction process is shown as follows (Eqs. 1-3):

$$h^+ + H_2O \rightarrow \text{-}OH + H^+ \quad (1)$$

$$e^- + O_2 \rightarrow O_2^- \quad (2)$$

$$O_2^- + \text{-}OH + H^+ \rightarrow H_2O + O_2 \quad (3)$$

As shown in Fig. 2A, the photocurrent responses of the CBFO-FTO electrode (red line) and the bare FTO electrode (black line) were recorded when platinum wire was used as the counter electrode. It can be seen the PEC response of the bare FTO electrode is rather small and can almost be negligible. Besides, it can be observed that the photocurrent response of the CBFO-FTO electrode is small when a platinum wire is used as the counter electrode.

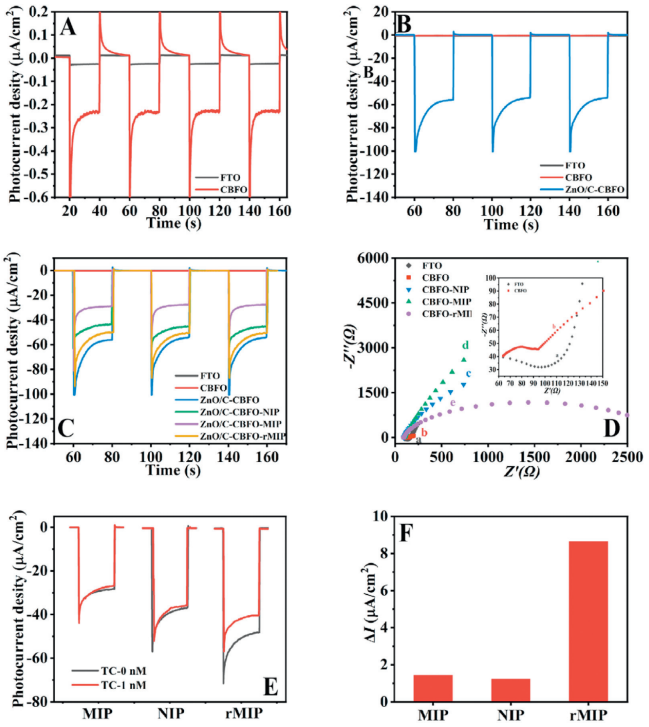

Fig. 2. (A) Photocurrent responses of the control and CBFO modified FTO electrodes with Pt electrode as counter electrode. (B) Photocurrent responses of the control and CBFO modified FTO electrodes with Pt electrode as counter electrode) and the CBFO modified FTO electrode with the ZnO/C modified FTO electrode as counter electrode. (C) Photocurrent response of the photocathodes modified with different materials. (D) Nyquist diagram of electrochemical impedance spectra (EIS) obtained at the photocathodes modified with different materials: (a) FTO, (b) CBFO, (c) CBFO–NIP, (d) CBFO-MIP and (e) CBFO-rMIP. (E) Photocurrent response diagram of different modified electrodes in Na_2SO_4 solution (black line) and TC solution (red line). nM = nmol/L. (F) Photocurrent differences of different electrodes in Na_2SO_4 solution and TC solution.

This phenomenon indicates that the photoelectron transfer rate of CBFO material is not very fast.

Fig. 2B shows the photogenerated current signals generated by the cathode system with different electrodes as counter electrodes and the CBFO-FTO electrodes as working electrodes. When a Pt wire is used as the counter electrode, a small photocurrent signal less than 1 μA can be obtained. Moreover, a well-defined photocurrent peak with an intensity of about 60 μA can be observed when replacing the Pt wire with the ZnO/C-FTO electrode. This means that the proposed sensor can exhibit an excellent sensitivity when using the change of photocurrent as the output signal. It can be explained by the fact that more holes can be collected at the photocathode by using the ZnO/C based photoanode as the counter electrode compared to Pt electrode.

As shown in Fig. 2C, photocurrent characteristics are used to verify the photocathode sensing process with the ZnO/C-FTO electrode as the counter electrode. Compared with the photocurrent of the CBFO-FTO electrode, the photocurrent of CBFO/MIP-FTO electrode is much lower, which may be due to the steric hindrance effect caused by the favorable host-guest interaction between the MIP materials and TC on the CBFO-FTO electrode surface, which impedes the electron transfer process. By removing the template molecular (TC) in the MIP materials, the specific recognition sites for TC can be generated. Consequently, the photocurrent of the CBFO/rMIP-FTO electrode is obviously larger than that of the CBFO/MIP-FTO electrode, and is comparable to that of the CBFO/NIP-FTO electrode.

Electrochemical impedance spectroscopy (EIS) is an effective method to investigate the capability of electron transfer on the

electrode surface. The EIS characterization was carried out in an electrolyte solution (containing 0.1 mol/L KCl and 0.1 mmol/L $K_3[Fe(CN)_6]$ and 1 nmol/L $K_4[Fe(CN)_6]$) with an Ag/AgCl electrode used as the reference electrode, and the obtained results are shown in Fig. 2D. The charge transfer resistance (RCT) was represented by the high-frequency semicircular region of the Nyquist diagram. Compared to the bare and CBFO modified FTO electrode, the RCT value reaches the maximum after the modification of CBFO/MIP (curve d), which is due to the poor conductivity of *o*-PD and TC, impeding electron transfer. After removing the template molecular TC, the value of RCT decreases (curve e) and is comparable to that of the CBFO/NIP modified FTO electrode (curve c), confirming the successful removal of the template molecular.

Furthermore, the photocurrent responses of different electrodes to TC are shown in Fig. 2E. All three electrodes exhibit favorable responses to visible light, and a remarkable decrease in the photocurrent intensities can be observed at the CBFO-rMIP modified electrode in the present of TC, while just the slight changes of photocurrent intensity are obtained at other two electrodes (Fig. 2F). This can be attributed to the removal of the template molecules from the CBFO/rMIP modified electrode, thus leaving a greater number of cavities for photoelectron transport. These cavities can be reoccupied after the interaction with TC, thus resulting in an obvious decrease in the photocurrent signal. The results illustrate the successful construction of molecularly imprinted PEC sensors.

In the synthesis of CBFO/rMIP-FTO experiment part, CBFO/MIP-FTO was immersed into the elution solution to obtain CBFO/rMIP-FTO. The elution solution was composed of methanol and acetic acid at the ratio of 9:1 (v:v). As shown in Fig. S8A (Supporting information), by changing the soaking time of the CBFO/MIP-FTO electrode in elution solution, the difference photocurrent between the CBFO/MIP-FTO and CBFO/rMIP-FTO electrodes was obtained. The photocurrent difference increased first and then decreased with time, and reached the maximum at 5 min that is the optimal elution time. The reason for the largest current difference after 5 min elution may be that *o*-PD is also eluated after TC template elution, so that CBFO/MIP-FTO electrode returned to the state before polymerization. The explanation is as follow: When the CBFO/MIP-FTO electrode is soaked in the eluent, the functional bond between *o*-PD and tetracycline molecules will be destroyed firstly, resulting in the shedding of tetracycline molecules, which will lead to the increase of the photocurrent difference before and after soaking. When the tetracycline molecules are all elution, the photocurrent difference reaches the maximum, and the soaking time is 5 min. When the soaking time is prolonged, the eluent will break the functional bond between *o*-PD, causing *o*-PD to fall off, and the photocurrent difference will decrease.

In the adsorption test experience part, the CBFO/rMIP-FTO electrode was immersed in the TC solution to capture the template molecules, and the difference between the photocurrent intensities before and after capturing template molecules was obtained. As shown in Fig. S8B (Supporting information), the immersion time of the CBFO/rMIP-FTO electrode in the TC solution is changed to obtain the difference of photocurrent at different time. When the immersion time is in the range of 1–2 min, the photocurrent difference increases rapidly from 3 μA to 9 μA. After soaking for 2 min, the photocurrent difference remains almost constant due to the adsorption saturates. Therefore, the immersion time of 2 min was selected for the following experiments.

In order to evaluate the quantitative analysis performance of the CBFO/rMIP modified sensor, the photocurrent intensities of the TC solutions with varying concentrations were measured. As shown in Fig. 3A, in the concentration range of 0.01–10^5 nmol/L, the photocurrent signal gradually decreased with the increase of the TC concentration, indicating that the enhanced steric hindrance induced by the interaction between MIPs and the template molecules that hinder the electron transfer on the electrode surface. As illustrated in Fig. 3B, the photocurrent difference has a linear relationship with the logarithmic value of TC concentration, and the corresponding linear regression equation is $\Delta I = 2.5937\log CTC + 8.3941$ ($R^2 = 0.9951$). The limit of detection (LOD) of the sensor is calculated according to the following formula (Eq. 4):

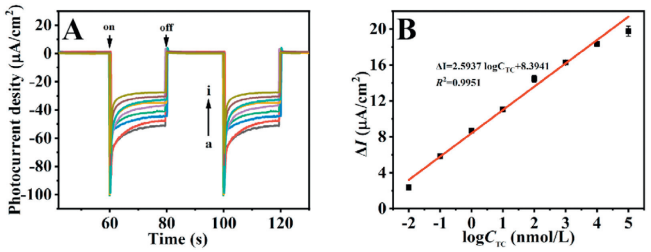

Fig. 3. (A) Photocurrent responses of the CBFO/rMIP modified sensor to TC in the concentration range from 0.01 nmol/L to 10^5 nmol/L with a stepwise increase by 10. The curve was the baseline. (B) Corresponding calibration curve of the CBFO/rMIP modified sensor for the TC determination.

Table 1
Comparison of different methods for TC determination.

Analytical method	Linear range (nmol/L)	Detection limit (nmol/L)	Ref.
ECL	1.0 - 1.0 × 10^5	0.47	[48]
Fluorescence	100 - 2.0 × 10^4	80	[14]
PEC	200 - 1.0 × 10^6	10	[49]
PEC	1.0 - 1.0 × 10^3	0.33	[50]
MIP-EC	5 - 500	0.85	[51]
MIP-PEC	0.01 - 1.0 × 10^5	0.007	This work

$$\mathrm{LOD} = 3S_B/m \quad (4)$$

where S_B represents the standard deviation of the PEC sensor in blank Na_2SO_4 solution; m represents the slope of the linear calibration curve [47]. The LOD is calculated to be 0.007 nmol/L. The comparison of the proposed PEC sensing method with other methods for determination of TC is summarized in Table 1 [14,48-51]. As illustrated, The PEC sensor has a more comprehensive linear range and a lower detection limit, which confirms that this analytical technique has a good application prospect in the high-sensitivity monitoring of antibiotics in food and environment.

To evaluate the stability of the proposed PEC sensor, the photocurrent response was continuously recorded after 50 on/off irradiation cycles for 1000 s, and the results are shown in Fig. S8A. As illustrated, the sensing platform with the ZnO/C modified eletrode as photoanode and the CBFO/rMIP modified electrode as photocathode exhibits a favorable stability. Fig. S8B reflects the photocurrent of six batches of the CBFO/rMIP-FTO electrodes after TC detection. It can be seen that no obvious difference in the photocurrent intensity is found for different batches of the CBFO/rMIP-FTO electrodes, indicating the good repeatability of the proposed PEC sensor. To verify the specific capture of TC by the molecular imprinted PEC sensor, interference experiments of other antibiotics were performed, and the obtained results are shown in Figs. S8C and D (Supporting information). Several antibiotics (*i.e.*, oxytetracycline (OTC), chloramphenicol (CAP), kanamycin (KAN), erythromycin (ERY) and chlortetracycline (CTC)) were selected as the interfering substances. The results demonstrate that the proposed PEC sensor exhibits the best detection performance to TC compared to other antibiotics, and the presence of these antibiotics have no impact on the photocurrent response to TC, suggesting the satisfactory selectivity of the PEC sensor.

In order to investigate the feasibility of the sensor for determination of TC in milk samples, the standard addition method

Table 2
Determination of TC in different spiked milk samples with different concentrations.

Sample	Concentration added (nmol/L)	Found (nmol/L)	Recovery (%)	RSD (%, $n = 3$)
1	0.1	0.093	93.11	2.74
2	10	11.04	110.47	2.75
3	100	108.17	108.17	2.11

was selected to evaluate the accuracy of the constructed PEC sensor. The TC solutions with gradient concentrations (0, 0.1, 10, 100 nmol/L) were added to the milk samples, and each sample was determined independently for 3 times. As shown in Table 2, the recoveries are found to be ranged from 93.1% to 110.5% with RSD ranged from 2.1% to 2.7%. In addition, an additional sample of environmental wastewater was selected, and the PEC sensor achieved the same satisfactory results. The results demonstrate the practicability and accuracy of the self-powered molecularly imprinted PEC sensor for practical sample testing.

In summary, a self-powered photochemical molecularly imprinted sensor integrated the ZnO/C photoanode and the CBFO photocathode for TC detection was prepared successfully. Without the external bias, the photoelectric signal of the CBFO photocathode was amplified by the ZnO/C photoanode. Furthermore, specific TC recognition sites were integrated into this self-powered sensor to improve its specificity to the target molecule. The constructed sensor has a wide linear range of 0.01-1.0 $\times$ 10^5 nmol/L and a LOD as low as 0.007 nmol/L. In addition, the sensor displays the satisfactory selectivity, reproducibility and stability. Predictably, this self-powered molecularly imprinted PEC sensing platform will show great potential in the detection of antibiotics in environment and foods.

Declaration of competing interest

The authors declare that they have no known competing financial interests or personal relationships that could have appeared to influence the work reported in this paper.

CRediT authorship contribution statement

Qinghong Pan: Writing – original draft, Investigation, Formal analysis, Data curation. **Huafang Zhang:** Investigation, Data curation. **Qiaoling Liu:** Writing – original draft, Validation, Supervision. **Donghong Huang:** Methodology, Formal analysis. **Da-Peng Yang:** Writing – review & editing, Validation, Supervision, Resources, Project administration, Methodology, Investigation, Funding acquisition, Formal analysis, Conceptualization. **Tianjia Jiang:** Software, Investigation, Formal analysis. **Shuyang Sun:** Project administration. **Xiangrong Chen:** Writing – review & editing, Project administration, Funding acquisition.

Acknowledgments

This work was supported by the Fuxiaquan Collaborative Innovation Platform (No. K30001), Major Scientific Research Program for Young and Middle-aged Health Professionals of Fujian Province, China (No. 2022ZQNZD007), Youth Innovation Technology Project of Higher School in Shandong Province (Food Nanotechnology Innovation Team).

Supplementary materials

Supplementary material associated with this article can be found, in the online version, at doi:10.1016/j.cclet.2024.110169.

References

[1] M.L. Cui, Z.X. Lin, Q.F. Xie, et al., Food Chem. 412 (2023) 135554.
[2] G. Shi, C. Yan, J. Chen, Biosens. Bioelectr. 228 (2023) 115188.
[3] Z. Pan, W. Ding, H. Chen, H. Ji, Chin. Chem. Lett. 35 (2024) 108567.
[4] R. Xu, Z. Shen, Y. Xiang, et al., Biosens. Bioelectr. 220 (2023) 114785.
[5] C. Feng, J. Zhang, C. Bian, et al., Chin. Chem. Lett. 34 (2023) 108457.
[6] Q. Du, P. Wu, Y. Sun, et al., Chem. Eng. J. 390 (2020) 124614.
[7] S. Zhang, Q. Sun, X. Liu, et al., Sens. Actuators B: Chem. 372 (2022) 132687.
[8] Z. Li, F. Meng, R. Li, et al., Biosens. Bioelectr. 234 (2023) 115294.
[9] Z. Hu, Y. Xu, H. Wang, et al., Chin. Chem. Lett. 33 (2022) 4750–4755.
[10] X. Wang, G. Xing, N. Li, et al., Chin. Chem. Lett. 34 (2023) 108110.
[11] H. Xu, H.Y. Mi, M.M. Guan, et al., Food Chem. 232 (2017) 198–202.
[12] X. Li, Y. Jia, J. Zhang, et al., Chin. Chem. Lett. 33 (2022) 2105–2110.
[13] T.X. Chen, F. Ning, H.S. Liu, et al., Chin. Chem. Lett. 28 (2017) 1380–1384.
[14] C.Y. Wang, C.C. Wang, X.W. Zhang, et al., Chin. Chem. Lett. 33 (2022) 1353–1357.
[15] X. Ai, Y.H. Li, Y.W. Li, et al., Chin. Chem. Lett. 33 (2022) 2832–2844.
[16] M. Ramya, P. Senthil Kumar, G. Rangasamy, et al., Chemosphere 308 (2022) 136416.
[17] X. Liu, Y. Zhao, F. Li, Biosens. Bioelectr. 173 (2021) 112832.
[18] H. Xue, J. Zhao, Q. Zhou, et al., ACS Appl. Nano Mater. 2 (2019) 1579–1588.
[19] Z. Cui, Z. Li, Y. Jin, et al., Food Chem. 328 (2020) 127063.
[20] H. Kaur, S.S. Siwal, G. Chauhan, et al., Chemosphere 304 (2022) 135182.
[21] B. Zhang, H. Wang, J. Xi, F. Zhao, B. Zeng, ACS Sens. 5 (2020) 2876–2884.
[22] T. Wu, J. Feng, S. Zhang, et al., Biosens. Bioelectr. 169 (2020) 112580.
[23] G.C. Fan, Y. Lu, H. Zhao, et al., Biosens. Bioelectr. 137 (2019) 52–57.
[24] H. Xiong, Y. Wan, Y. Fan, et al., Chin. Chem. Lett. 35 (2024) 108382.
[25] Q. Chen, C. Yuan, C. Zhai, Chin. Chem. Lett. 33 (2022) 983–986.
[26] J. Wang, J. Bei, X. Guo, et al., Biosens. Bioelectr. 208 (2022) 114220.
[27] Q. Liu, H. Zhang, H. Jiang, et al., Biosens. Bioelectr. 216 (2022) 114634.
[28] K. Yan, P. Karthick Kannan, D. Doonyapisut, et al., Adv. Funct. Mater. 31 (2020) 2008227.
[29] C. Wu, X. Luo, X. Yu, et al., Chin. Chem. Lett. 34 (2023) 107881.
[30] F. Yin, E. Yang, X. Ge, et al., Chin. Chem. Lett. 35 (2024) 108753.
[31] S. Verma, P. Arya, A. Singh, et al., Biosens. Bioelectr. 165 (2020) 112347.
[32] M. Xiao, M. Zhu, R. Yuan, Y. Yuan, Biosens. Bioelectr. 227 (2023) 115151.
[33] C. Li, J. He, Y. Xiao, Y. Li, J.J. Delaunay, Energy Environ. Sci. 13 (2020) 3269–3306.
[34] D. Kang, J.C. Hill, Y. Park, K.S. Choi, Chem. Mater. 28 (2016) 4331–4340.
[35] M. Huang, C. Zhou, J. Tian, et al., Biosens. Bioelectr. 165 (2020) 114357.
[36] S. Li, Q. Zhou, Z. Li, M. Liu, Y. Li, Chin. Chem. Lett. 35 (2024) 108693.
[37] H. Tong, C. Cao, M. You, et al., Biosens. Bioelectr. 213 (2022) 114449.
[38] Z. Bie, R. Xing, X. He, et al., Anal. Chem. 90 (2018) 9845–9852.
[39] S.X. Zhou, X.T. Lin, J. Wang, H.X. Wang, G.T. Chen, Food Chem. 421 (2023) 136196.
[40] Y.Z. Zhang, B. Zhang, Q.Q. Chen, et al., Food Chem. 424 (2023) 136133.
[41] Y. Zhao, R. Wang, Y. Wang, G. Jie, H. Zhou, Food Chem. 413 (2023) 135627.
[42] Y. Li, C. Liu, Q. Li, S. Mao, Chin. Chem. Lett. 35 (2024) 109541.
[43] H. Zhang, Z. Kang, H. Zhu, H. Lin, D.P. Yang, Sci. Total Environ. 859 (2023) 160284.
[44] K. Lu, C. Hong, D. Liu, et al., Sens. Actuators B: Chem. 371 (2022) 132588.
[45] Y. Yang, W. Yan, X. Wang, et al., Biosens. Bioelectr. 177 (2021) 113000.
[46] X. Dong, Z. Shi, C. Xu, et al., Biosens. Bioelectr. 149 (2020) 111843.
[47] L. Mao, K. Ji, L. Yao, et al., Biosens. Bioelectr. 127 (2019) 57–63.
[48] D. Jiang, M. Wei, X. Du, et al., Biosens. Bioelectr. 200 (2022) 113917.
[49] Q. Han, R. Wang, B. Xing, et al., Biosens. Bioelectr. 106 (2018) 7–13.
[50] M. Guo, R. Wang, Z. Jin, et al., ACS Appl. Polym. Mater. 4 (2022) 1234–1242.
[51] Y. Chen, Y. Xia, Y. Liu, et al., Biosens. Bioelectr. 216 (2022) 114650.